Expert Systems with Applications 39 (2012) 3423–3431

Contents lists available at SciVerse ScienceDirect

Expert Systems with Applications

journal homepage: www.elsevier.com/locate/eswa

# A novel extension neural network based partial discharge pattern recognition method for high-voltage power apparatus

Hung-Cheng Chen *, Feng-Chang Gu, Meng-Hui Wang

*Department of Electrical Engineering, National Chin-Yi University of Technology, Taiwan*

ARTICLE INFO

*Keywords:*
Extension neural network
Fractal feature
Partial discharge
Pattern recognition
Extension distance

ABSTRACT

This paper proposes a novel partial discharge (PD) pattern recognition method based on extension neural network (ENN) using fractal features. Five types of defect models are well-designed on the base of investigation of power apparatus failures. A PD detector is used to measure the raw three-dimension (3D) PD patterns, from which the fractal dimension, the lacunarity, and the mean discharges of phase windows are extracted as PD features. These critical features form the cluster domains of defect types. An ENN is then developed to recognize the pattern of partial discharge, which utilizes an extension distance (ED) instead of Euclidean distance to measure the similarities among the recognized data and the cluster domains. The ENN with simpler structure than traditional neural networks is capable of processing the clustering problems which have a range of feature values, supervised learning, continuous input, and descriptive output. Moreover, the ENN has the advantages of higher accuracy, shorter learning times, and noise tolerance, which are useful in recognizing the PD patterns of electrical apparatus. To demonstrate the effectiveness of the proposed method, comparative studies among multilayer neural network (MNN), extension theory, and K-means are conducted on 200 sets of field-test PD patterns with rather encouraging results.



## 1. Introduction

Partial discharge measurement has been widely application in insulation diagnosis for high-voltage power apparatus, such as XLPE power cable (Okabe, Kaneko, Minagawa, & Nishida, 2008; Yue et al., 2006), gas insulated switchgear, and power transformers. The purpose of the insulation diagnosis for power apparatus is to give system operators the information on dielectric deterioration degree of high-voltage equipment. The main parameters of the 3D PD patterns are phase angle $\phi$, discharge magnitude $q$, and the number of discharge $n$. Using the PD detector to measure the signal of electrical or magnetic field variation caused by the PD in defect power equipment, the information about these quantities have become obtainable, precise, and detailed. Each type of defect can be characterized by the shape of the 3D pattern. Therefore, an expert can utilize the pattern recognition to identify the different defect types in accordance with the 3D patterns.

Fractal has been very successfully used in description of naturally occurring phenomena and complex shape (Ruello et al., 2010; Wu et al., 2010), such as mountain ranges, coastlines, clouds, and so on, wherein traditional mathematics were found to be inadequate. PD also is a natural phenomenon occurring in electrical insulation systems, which invariably contain tiny defects and non-uniformities, and gives rise to a variety of complex shapes and surfaces, both in a physical sense as well as in the shape of 3D PD patterns acquired using PD detector. This complex nature of the PD pattern shapes and the ability of fractal geometry to model complex shapes, are the main reasons which encouraged the authors to make an attempt to study its feasibility for PD pattern interpretation.

Various pattern recognition techniques, including fuzzy clustering (Li, 2009; Li, Liao, Grzybowski, & Yang, 2010) and neural network (NN) (Karthikeyan, Gopal, & Venkatesh, 2008; Karthikeyan, Gopal, & Vimala, 2005), have been extensively used in PD recognition. The fuzzy approaches require human expertise and have been successfully applied to this field. However, there are difficulties in acquiring knowledge and in maintaining the database. The main advantage of the NN can directly acquire experience from the training data. However, the training data must be sufficient to describe a status. Another limitation of the NN approach is the inability to use linguistically descriptive output, because it is difficult to understand the content of network.

To improve the performances of traditional clustering methods, an extension neural network (ENN) (Wang & Hung, 2003; Wang, 2005; Lay et al., 2008) based clustering method is proposed for the PD pattern recognition of high-voltage power apparatus in this

* Corresponding author. Address: 35, Lane 215, Sec. 1, Chungshan Rd., Taiping, Taichung 411, Taiwan. Tel.: +886 423924505; fax: +886 423924419.
*E-mail address:* hcchen@ncut.edu.tw (H.-C. Chen).

0957-4174/$ - see front matter © 2011 Elsevier Ltd. All rights reserved.
doi:10.1016/j.eswa.2011.09.030

article. The fractal features, fractal dimension and lacunarity, and the mean discharges are extracted from the raw 3D PD patterns to highlight the more detailed characteristics of PD. These three features are selected as the input variables of the ENN. The ENN utilizes an extension distance instead of Euclidean distance (ED) to measure the similarities among the tested data and the cluster domain. It can quickly and stably learn to categorize input patterns and permit adaptive processes to access new significant information. Moreover the ENN has shorter learning times and a simpler structure than traditional MNN. To demonstrate the effectiveness of the ENN-based recognition method, 200 sets of field-test PD patterns are tested. The results show that the ENN-based recognition method is suitable as a practical solution for PD pattern recognition.

## 2. Theory of the ENN

The ENN is a new topology of neural network, which combines extension theory (Cai, 1983; Wang, Tseng, Chen, & Chao, 2009) and neural network. The extension theory provides a novel distance measurement for classification and the NN can embed the salient features of parallel computation power and learning capability. The ENN is capable of processing the clustering problems which have a range of feature values, supervised learning, continuous input, and descriptive output.

### 2.1. Structure of the ENN

In PD pattern recognition, the PD features of the associated defect types cover a range of values. Therefore, the ENN is appropriate for PD recognition. Fig. 1 shows the schematic structure of the ENN. It consists of the input layer and the output layer. There are two connection values called weights between each input node and each output node, one represents the upper bound of the classical domain of the feature, the other represents the lower bound. The lower bound and the upper bound of the weight between the $j$th input node and the $k$th output node are denoted by $w_{kj}^L$ and $w_{kj}^U$, respectively. All the weights of an ENN are adjusted by performing a proposed learning algorithm on input features. The output layer is a competitive layer. There is one node in the output layer for each prototype pattern, and only one output node with nonzero output to indicate the prototype pattern that is closest to the input vector. The operation modes of an ENN can be separated into the learning phase and the operation phase, which are discussed in the next section.

### 2.2. Learning algorithm of the ENN

The learning algorithm of the ENN is essential a supervised learning which tunes the weights of the ENN to achieve good clustering performance or minimize the clustering error. Before learning, several variables have to be defined. Training data set to be $X = \{X_1, X_2, \ldots, X_{N_s}\}$, where $N_s$ is the total number of training patters. The $i$th training pattern is $X_i^p = \{x_{i1}^p, x_{i2}^p, \ldots, x_{in}^p\}$, where $n$ is the total number of features, and $p$ is the category of $i$th pattern. To evaluate the clustering performance, if $N_e$ is total error number, then the total error rate $E_r$ can be defined as

$$E_r = \frac{N_e}{N_s} \tag{1}$$

The supervised learning algorithm of ENN is explicitly described as follows (Wang, 2005):

**Step 1.** Set the connection weights between input node and output node by the matter-element model

$$R_k = \begin{bmatrix} \text{cluster } k, & c_1 & V_{k1} \\ & c_2 & V_{k2} \\ & \vdots & \vdots \\ & c_j & V_{kj} \\ & \vdots & \vdots \\ & c_n & V_{kn} \end{bmatrix} \tag{2}$$

where $k = 1,2,\ldots,m$ and $j = 1, 2,\ldots,n$. $m$ is the total number of cluster and $n$ is the total number of features. $c_j$ is the $j$th feature of the cluster $k$, and $V_{kj} = \langle w_{kj}^L, w_{kj}^U \rangle$ is the classical domain of cluster $k$. Let $T_i$ is the corresponding target output of the $i$th training pattern $X_i$. The weights of training pattern can be determined as follows:

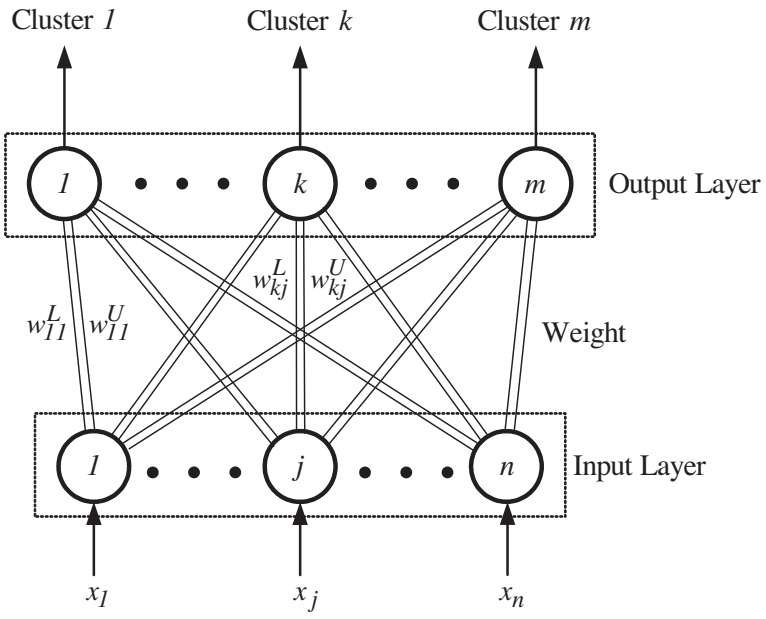


**Fig. 1.** Structure of the extension neural network (ENN).

$$w_{kj}^{L} = \min_{T_i \in k}(x_{ij}) \tag{3}$$

$$w_{kj}^{U} = \max_{T_i \in k}(x_{ij}) \tag{4}$$

for $i = 1,2,\ldots,N_s$, $j = 1,2,\ldots,n$, and $k = 1,2,\ldots,m$.

**Step 2.** Calculate the initial weight centers of each cluster defined as

$$w_{cen,kj} = \frac{w_{kj}^{U} + w_{kj}^{L}}{2} \tag{5}$$

**Step 3.** Read the $i$th training pattern and its cluster number $p$

$$X_i^p = \{x_{i1}^p, x_{i2}^p, \ldots, x_{in}^p\} \tag{6}$$

where $p \in m$.

**Step 4.** Calculate the extension distance, the distance between the input pattern $X_i$ and the $k$th cluster, as follows (Wang, 2005:

$$ED_{ik} = \sum_{j=1}^{n} \left( \frac{|x_{ij} - w_{cen,kj}| - \frac{w_{kj}^{U} - w_{kj}^{L}}{2}}{\frac{w_{kj}^{U} - w_{kj}^{L}}{2}} + 1 \right)$$
$$\text{for } k = 1,2,\ldots,m. \tag{7}$$

The extension distance can be graphically presented as Fig. 2. The ED can characterize the distance between $x$ and a range of $\langle w^L, w^U \rangle$. We can observe that different ranges of classical domains can arrive at different distances. This is a significant advantage in classification application. Usually, if the feature covers a small range, the data precision requirement is high sensitive to distance.

**Step 5.** Find the $b$, such that $ED_{ib} = \min\{ED_{ik}\}$. If $b$=$p$, then go to Step 7; Otherwise, go to Step 6.

**Step 6.** Update the weights of $p$th and $b$th clusters as follows:

(a) Update the cluster center

$$w_{cen,pj}^{new} = w_{cen,pj}^{old} + \eta(x_{ij} - w_{cen,pj}^{old}) \tag{8}$$

$$w_{cen,bj}^{new} = w_{cen,bj}^{old} - \eta(x_{ij} - ww_{cen,bj}^{old}) \tag{9}$$

(b) Update the $p$th and $b$th cluster

$$\begin{cases} w_{pj}^{L(new)} = w_{pj}^{L(old)} + \eta(x_{ij} - w_{cen,pj}^{old}) \\ w_{pj}^{U(new)} = w_{pj}^{U(old)} + \eta(x_{ij} - w_{cen,pj}^{old}) \end{cases} \tag{10}$$

$$\begin{cases} w_{bj}^{L(new)} = w_{bj}^{L(old)} - \eta(x_{ij} - w_{cen,bj}^{old}) \\ w_{bj}^{U(new)} = w_{bj}^{U(old)} - \eta(x_{ij} - w_{cen,bj}^{old}) \end{cases} \tag{11}$$

where $\eta$ is a learning rate which is set to 0.1 in this paper. The learning process is only tuning weights of the $p$th and $b$th clusters.

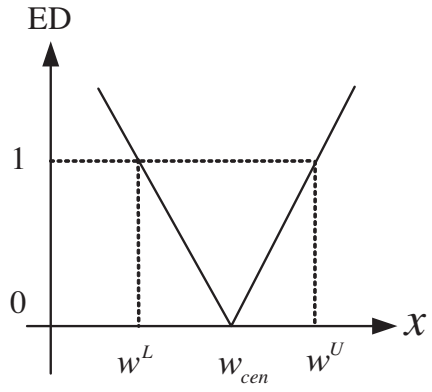


**Fig. 2.** Extension distance (ED).

**Step 7.** Repeat Step 2–6, if all patterns have been classified, then a learning epoch is finished.

**Step 8.** Stop, if the clustering process has converged, or the error has arrived at a preset value; Otherwise, return to Step 3.

The ENN can take human expertise before the learning, and it can also provide meaningful output after learning, because the classified boundaries of the features are clearly determined.

### 2.3. Operation phase of the ENN

**Step 1.** Read the weight matrix of the ENN.

**Step 2.** Read a testing pattern as

$$X_t = \{x_{t1}, x_{t2}, \ldots, x_{tn}\} \tag{12}$$

**Step 3.** Use the extension distance (ED) to calculate the distance between the testing pattern and each cluster by Eq. (5).

**Step 4.** Find the $b$, such that $ED_{ib} = \min\{ED_{ik}\}$, set the result is 1 to indicate the cluster of the tested pattern.

**Step 5.** Stop, if all of the tested patterns have been classified; otherwise, go to Step 2.

## 3. Extraction of PD features

Fractals have been very successfully used to address the problem of modeling and to provide a description of naturally occurring phenomena and shapes, wherein conventional and existing mathematical methods were found to be inadequate. In this theory, fractal dimensions are allowed to depict surface asperity of complicated geometric things. Therefore, it's possible to study complex objects with simplified formulas and fewer parameters (Satish & Zaeng, 1995). PD also is a natural phenomenon occurring in electrical insulation systems which invariably contain tiny defects and non-uniformities. It gives rise to a variety of complex shapes and surfaces, both in a physical sense as well as in the shape of 3D PD patterns acquired using digital PD detector (Chen, Gu, & Lee, 2008). Both the complex nature of the PD pattern shapes and the ability of fractal geometry to model complex shapes are the main reasons which encouraged the authors to make an attempt to study its feasibility for PD pattern interpretation.

The fractal features, fractal dimension and lacunarity, and the mean discharges of phase windows are extracted to highlight the more detailed characteristics of the raw 3D PD patterns. The extracted features in this paper are introduced as follows:

### 3.1. Fractal dimension

While the definition of fractal dimension by self-similarity is straightforward, it is often difficult to estimate/compute for a given image data. However, a related measure of fractal dimension, the box dimension, can be computed more easily. In this work, the method suggested by Voss, and others in Voss (1985), for the computation of fractal dimension D from the image data has been followed. Let $p(m,L)$ define the probability that there are $m$ points within a box of size $L$ (i.e. cube of side $L$), which is centered about a point on the image surface. $p(m,L)$ is normalized, as below, for all $L$

$$\sum_{m=1}^{N} p(m,L) = 1 \tag{13}$$

where $N$ is the number of possible points within the box. Let $S$ be the number of image points (i.e. pixels in an image). If one overlays the image with boxes of side $L$, then the number of boxes with $m$ points inside the box is $(S/m)p(m,L)$. Therefore, the expected total

number of boxes needed to cover the whole image (Mandelbrot, 1983) is

$$N(L) = \sum_{m=1}^{N} \frac{S}{m} p(m,L) = S \sum_{m=1}^{N} \frac{1}{m} p(m,L) \tag{14}$$

This value is also proportional to $L^{-D}$ and the box dimension $D$ can be estimated by calculating $p(m,L)$ and $N(L)$ for various values of $L$, and by doing a least square fit on $[\log(L), \log(N(L))]$. To estimate $p(m,L)$, one must center the cube of size $L$ around an image point and count the number of neighboring points $m$, that fall within the cube. Accumulating the occurrences of each number of neighboring points over the image gives the frequency of occurrence of $m$. This is normalized to obtain $p(m,L)$. Values of $L$ are chosen to be odd to simplify the centering process. Also, the centering and counting activity is restricted to pixels having all their neighbors inside the image. This obviously will leave out image portions of width = $(L-1)/2$on the borders. This reduced image is then considered for the counting process. As is seen, large values of $L$ results in increased image areas from being excluded during the counting process, thereby increasing uncertainty about counts near border areas of the image. This is one of the sources of errors for the estimation of $p(m,L)$ and thereby $D$. Additionally, the computation time grows with the $L$ value. Hence, $L = 3, 5, 7$, and 11 were chosen for this work. Fig. 3 shows a sample plot of the set $[\log(L), -\log(N(L))]$ for the different size $L$.

### 3.2. Lacunarity

Theoretically, ideal fractal could confirm to statistical similarity for all scales. In other words, fractal dimensions are independent of scales. However, it has been observed that fractal dimension alone is insufficient for purposes of discrimination, since two differently appearing surfaces could have the same value of $D$. To overcome this, Mandelbrot introduced the term called lacunarity $\Lambda$, which quantifies the denseness of an image surface. Many definitions of this term have been proposed and the basic idea in all these is to quantify the 'gaps or lacunas' present in a given surface. One of the useful definitions of this term as suggested by Chen et al. (2008) is

$$M(L) = \sum_{m=1}^{N} m p(m,L) \tag{15}$$

$$M^2(L) = \sum_{m=1}^{N} m^2 p(m,L) \tag{16}$$

where $N$ is the number of point in the data set of size $L$, the lacunarity becomes

$$\Lambda(L) = \frac{M^2(L) - [M(L)]^2}{[M(L)]^2} \tag{17}$$

Fig. 4 shows a sample plot of the variation of lacunarity with respect to box size $L$ (3, 5, 7, 9 and 11). Fig. 5 shows the procedure for extracting fractal features. In fractal dimension extraction the first step is to transfer PD pattern to a $512 \times 512$ matrix. $N(L)$ is then obtained by using different box size L. Finally fitting the data $[\log L, -\log(N(L))]$ can obtain fractal dimension. In lacunarity extraction, the first step is to transfer PD pattern to a binary image $512 \times 512$ matrix. Then the chosen box size is $L = 3$, which is the best box size for the computation of the $M(L)$ and $M^2(L)$. Finally, the lacunarity can be obtained by Eq. (17).

### 3.3. Mean values of discharges

The detailed features extraction process of mean values of discharges is shown in Fig. 6. A 3D PD pattern is divided into ten phase windows whose width is set to 36°. The mean discharge is calculated in every phase window. We will obtain 10 mean discharge parameters on the whole 360° phase angles. If each phase window is further divided into $n \times m$ equal sections, the mean value of each phase window can be calculated by

$$v_i = \frac{\sum_{j=1}^{m} \sum_{k=1}^{n} q_j n_{jk}}{\sum_{j=1}^{m} \sum_{k=1}^{n} n_{jk}} \quad \text{for } i = 1, 2, \ldots, 10 \tag{18}$$

where $q_j$ is the discharge magnitude in $j$th row. $n_{jk}$ is the discharge number in $jk$th section.

## 4. PD recognition system design

The block diagram of the designed PD recognition system is shown in Fig. 7. It consists of three main parts: well-designed defect models, measurement system, and ENN-based recognition method. The details of the three main parts are introduced in subsequent paragraphs.

### 4.1. Defect model

According to the fact that gap discharge and surface discharge are more likely to occur in high-voltage power equipments, five types of relevant models are well-designed on the base of investi-

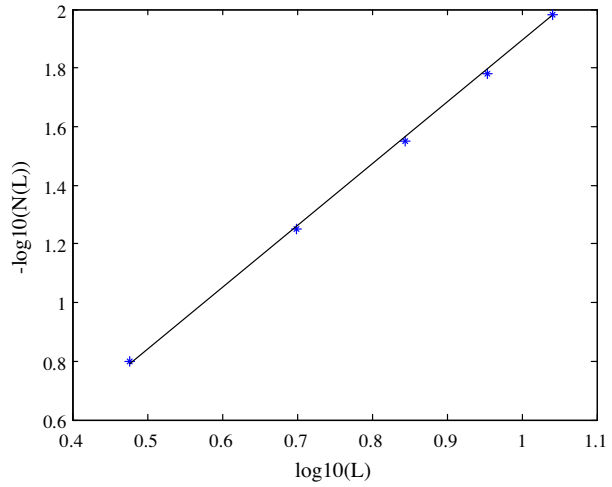


**Fig. 3.** Sample plot of the set $[\log(L), \log(N(L))]$ for different box size $L$.

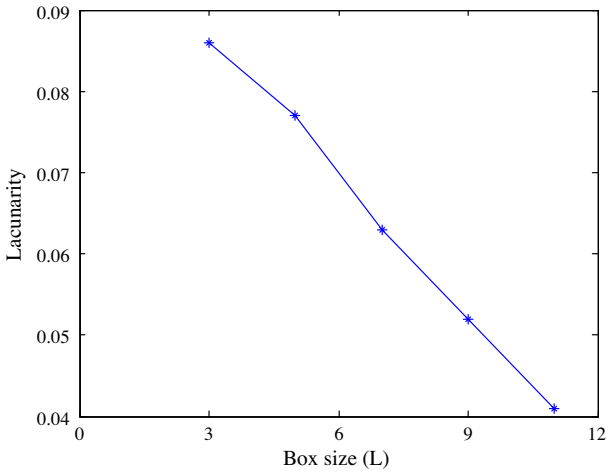


**Fig. 4.** Sample plot of the variation of lacunarity with respect to box size $L$.

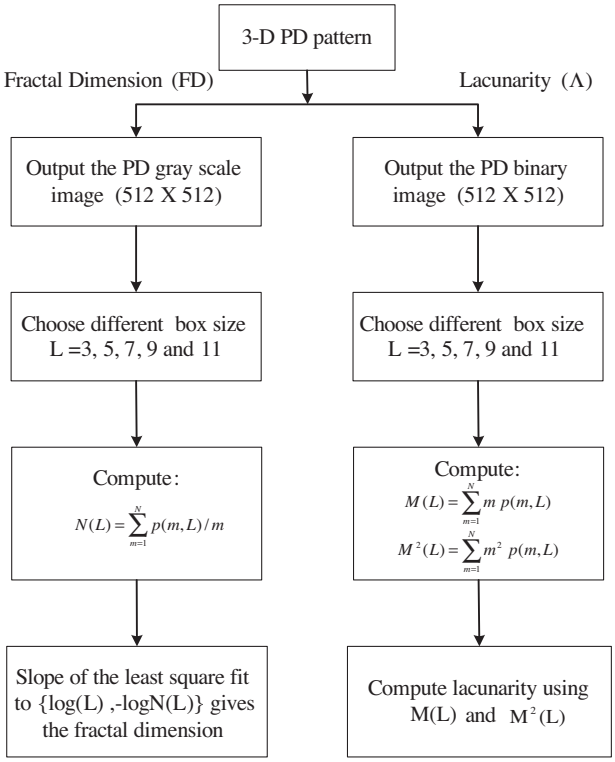


**Fig. 5.** Procedure for computing fractal dimension and lacunarity.

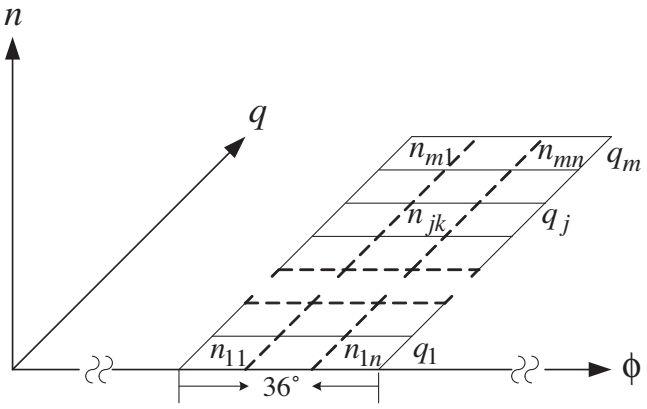


**Fig. 6.** Illustration for the calculation of mean values of charges.

gation of many power equipment failures to outline the features of PD.

T1: Plane to plane model. A 9 mm-in-thickness epoxy with a 3 mm-in-diameter cylindrical cavity is inserted.
T2: Plane to plane model. A 3 mm-in-thickness epoxy is inserted.
T3: Needle to plane model. A 4 mm-in-diameter copper stick is lathed at one end to a 30°, 0.5 mm-in-diameter cone needle which is 6 cm away from the plane.
T4: Needle to plane model. A 4 mm-in-diameter copper stick is lathed at one end to a 30°, 1 mm-in-diameter cone needle which is 6 cm away from the plane.
T5: Needle to plane model. A 4 mm-in-diameter copper stick is lathed at one end to a 30°, 2 mm-in-diameter cone needle which is 6 cm away from the plane.

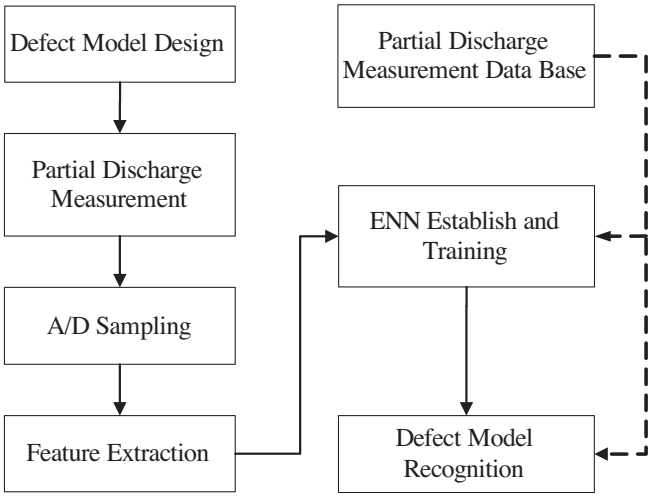


**Fig. 7.** Block diagram of the designed PD recognition system.

Both the plane and the needle are made of copper. The practical specimens of the defect models are shown in Fig. 8.

### 4.2. Measurement system

The structure of the measuring system is shown in Fig. 9. The autotransformer is used to slowly rise the output voltage of the transformer to 5.4 kV as the testing voltage on defect model. The detector LDP-5 equipped with a capacitive sensor measures the PD electrical signal generated by the defect model. The PD signal is converted into a computer by NI DAQ card (PCI-6110) for further analysis. For each type of defect model, 40 times measurements are conducted. The sampling rate of the PCI-6110 DAQ card is set to 2 M/s and data acquisition duration per measurement is 24 cycles (60 Hz). The acquired PD signal is transferred into a 3D pattern. The features of the 3D pattern are extracted and used as the input parameters of the recognition system base on ENN recognition method.

A man–machine interface for PD measurement is designed using LabVIEW. Analyzing the signal through LabVIEW can not only obtain the instant values of PD signal, but also compare to the testing voltage (60 Hz) in real time. The designed measurement man–machine interface is shown in Fig. 10. The red and green curves indicate the PD signal and the testing voltage waveform, respectively.

We used PD detector LDP-5 equipped with a capacitive sensor to measure the PD signal of the defect models. A typical PD impulse detected and manipulated by LDP-5 is shown in Fig. 11. The rise time is faster than fall time. The frequency of the impulse is about 30–40 kHz.

### 4.3. ENN-based recognition method

The flow chart of the proposed ENN-based recognition method is shown in Fig. 12. It is simply described as follows:

**Step 1:** Set up the training pattern. In training, we used twenty patterns for training in each defect type.
**Step 2:** Set up the structure of ENN that consists of twelve input nodes and five output nodes in this recognition system.
**Step 3:** Train the ENN using the proposed learning algorithm in Section 2.2.
**Step 4:** If the training process is finished then go to Step5; otherwise go to Step 3.
**Step 5:** Save the weight vector of the trained ENN.
**Step 6:** Use the trained ENN for pattern recognition.

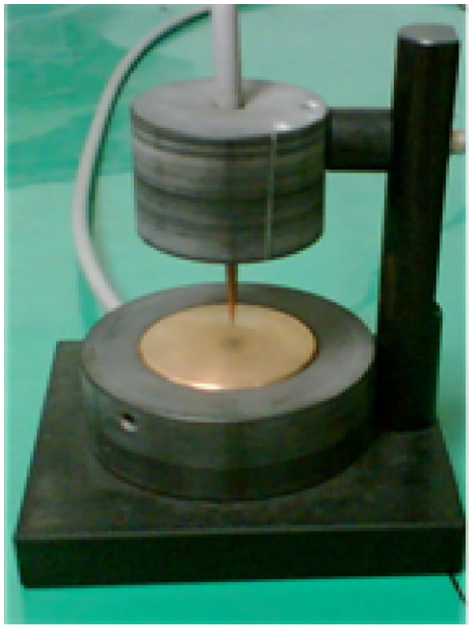

experimental object

9 mm-in-thickness epoxy with a 3 mm-in-diameter cylindrical cavity

0.5mm 1mm 2mm

4 mm-in-diameter copper stick is lathed at one end to a 30

3 mm-in-thickness epoxy

plane electrode

**Fig. 8.** Practical specimens of the defect model.

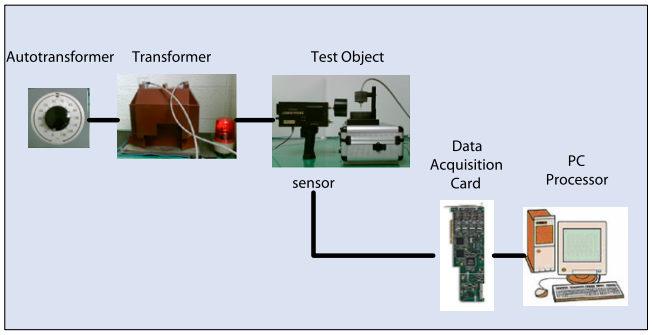


**Fig. 9.** Structure of the measurement system.

## 5. Experiment results and discussion

The proposed ENN-based recognition method has been implemented according to the measured PD pattern on the defect models. There are a total of 200 sets of measurement data associated with the five types of defect models. Some important experiment results are shown in the following.

### 5.1. 3D PD patterns

The typical 3D PD patterns transferred from the measured PD signals for each defect model are shown in Fig. 13. The main parameters of the 3D PD patterns are phase angle $\phi$, discharge

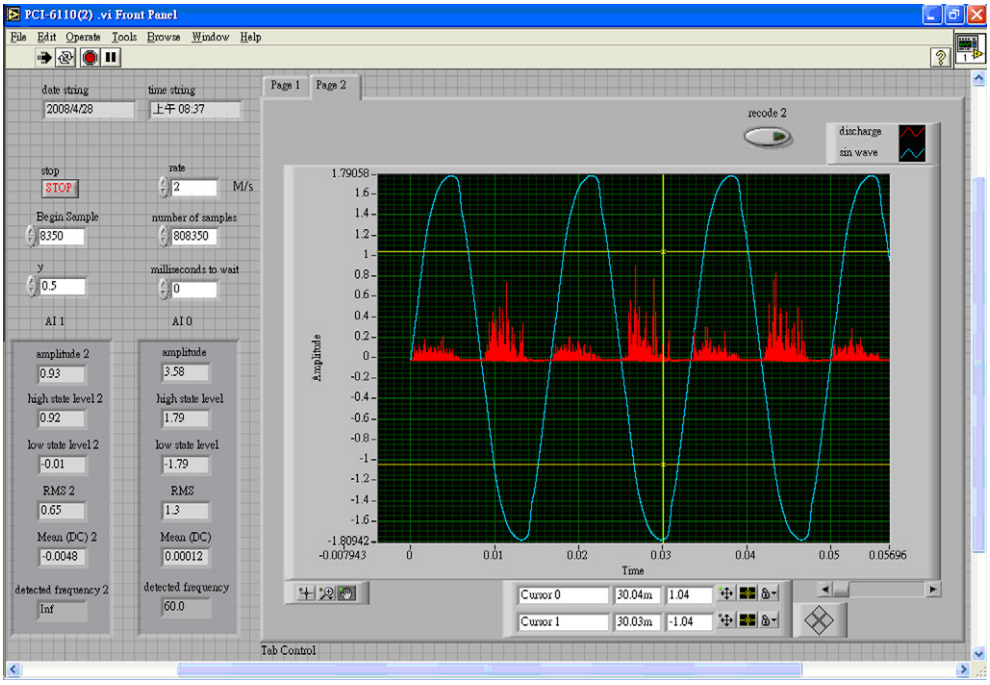


**Fig. 10.** Designed man–machine interface of PD measurement system.

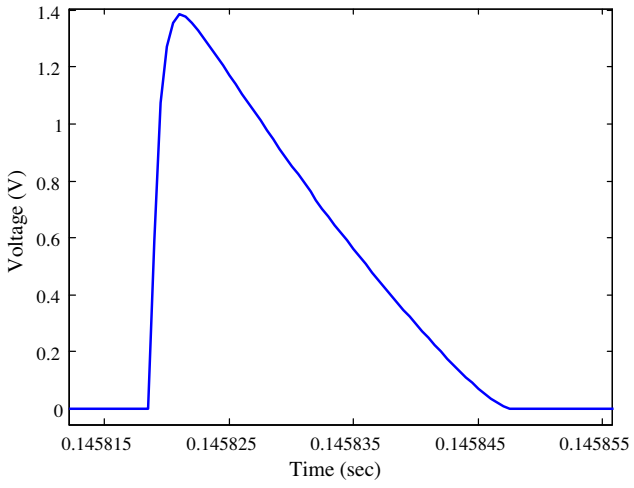


**Fig. 11.** PD impulse.

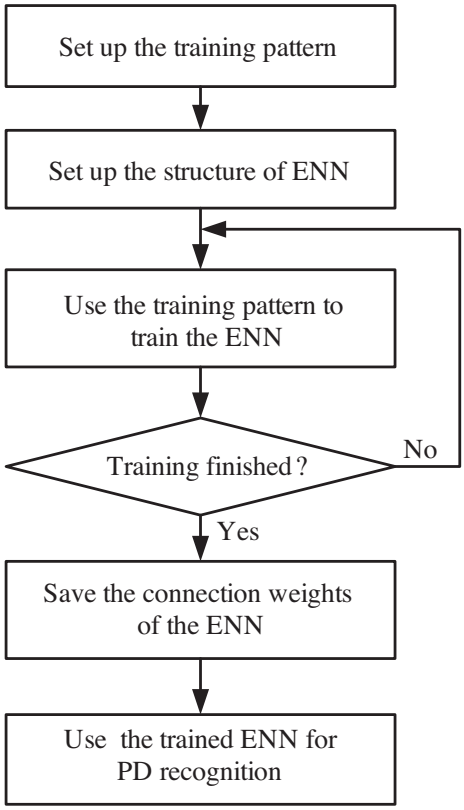


**Fig. 12.** Flow chart of the ENN-based recognition method.

magnitude $q$, and the numbers of discharge $n$. We can observe that the number of discharge in type T1 is less then in type T2, but distribution is wider than type T2. It is also very obvious that the numbers of discharge in types T3, T4, and T5 are greater than types T1 and T2. The discharges are happened more frequent when the needle-tip is thinner. The discharges of needle to plane model are almost happened in positive period. Sometimes types T3 and T4 have discharges happened in negative period, in which the number of discharge is few, but the discharge magnitude is large. According to the 3D PD pattern in each defect model we can find some different features between each defect model.

### 5.2. Feature extraction

The features of a total of 200 sets of 3D PD patterns are extracted and used as the input parameters of the recognition system base on ENN recognition method. Two features, the fractal dimension and the lacunarity, are calculated based on the fractal theory. The distribution of the fractal dimensions and the lacunarities of all 3D PD patterns is shown in Fig. 14. It is obvious that features belonging to a particular defect type gather together. According to these two fractal features type T1 and type T2 can be easily classified.

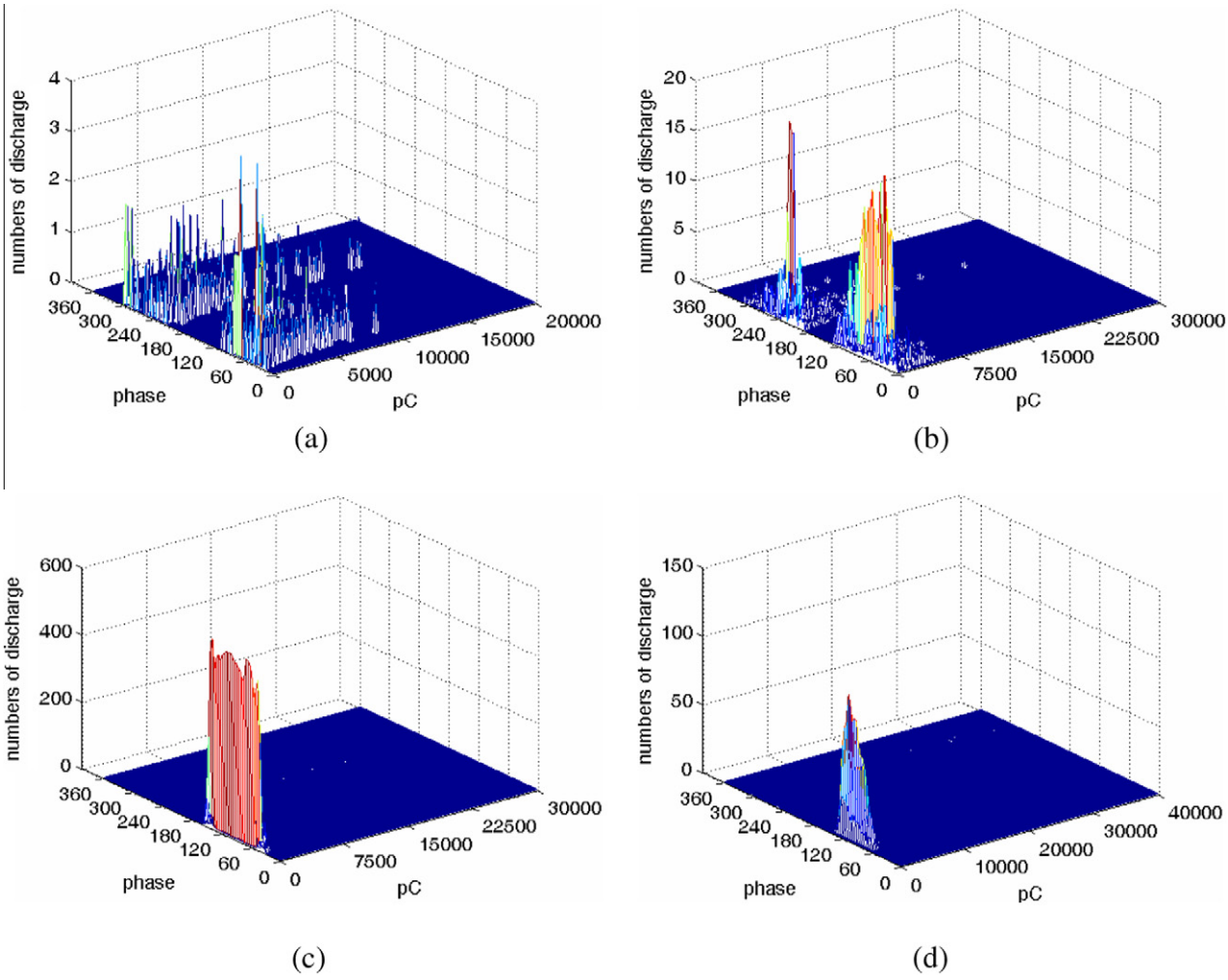


**Fig. 13.** Five typical defect type of 3D PD patterns: (a) type T1; (b) type T2; (c) type T3; (d) type T4; (e) type T5.

However, the distribution of type T3, T4, and T5 overlaps somewhere, which causes inaccurate classification. Therefore we take the mean values of discharge associated with phase windows as additional features. The mean discharges of all type of defect models associated with phase windows are shown in Fig. 15. We can find the distribution of T1 mean discharge magnitude is wider than the others. T4 mean discharge magnitudes in phase windows six to nine have the maximum discharge than the others. In Fig. 15 we can find there are many obvious differences in each defect type model.

### 5.3. Performance evaluation of the proposed ENN method

Table 1 shows the performance of the ENN method compared with the extension method, MNN, and K-means. We can find the K-means is the fastest than the others, but the recognition accuracy rates are the lowest. It should be noted that the structure of the ENN is very simple, only 120 connections are needed. Contrarily, the structure of the MNN needs 204 connections. Moreover the ENN recognition method also permits fast and adaptive processing for a large amount of training data, because the learning of ENN only requires tuning upper bounds and lower bounds of the excited connections. The ENN not only takes expert experience from learning, but also produces meaningful output after learning, because the optimal classified boundaries of the features are clearly determined. It can be seen from Table 1 that the ENN has a shorter than MNN. The

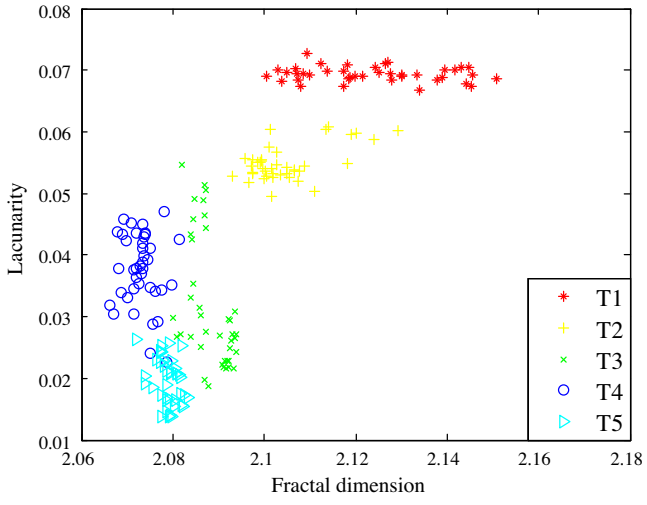


**Fig. 14.** Distribution of fractal features of all defect models.

number of learning epochs we set is less than 20, which only spends 0.11 s of CPU time. Compared with MNN, the MNN needs 1000 learning epochs in order to arrive at the target. It spends 105s CPU time because the MNN structure and the calculation are more

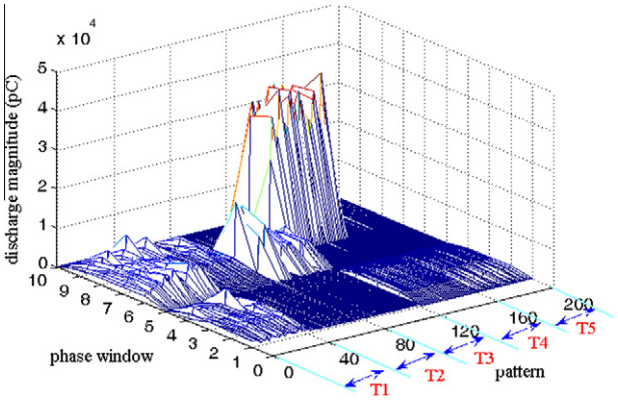


**Fig. 15.** Mean discharge magnitudes in phase windows.

**Table 1**
Performance comparison of the ENN method.

| Compared items | Diagnosis method | | | |
|---|---|---|---|---|
| | ENN method | Extension method | MNN | K-means |
| Structure | 12–5 | 12–5 | 12–12–5 | 12–5 |
| No. of connection | 120 | –[b] | 204 | –[b] |
| Learning epochs | ⩽20[a] | –[c] | 1000 | –[c] |
| CPU time (s) | 0.11 | 0.25 | 105 | 0.03 |

[a] ENN learning epochs is set less than 20 epochs.
[b] Connections between input and output are unnecessary.
[c] Learning epochs are unnecessary.

complicated. Although the PD recognition system is trained offline, the training time maybe is not a critical point to be evaluated. However, if we want to implement the PD recognition system in a microcomputer for a real-time PD detecting device or portable instrument, the performance of training would be important.

### 5.4. Recognition accuracy of the proposed ENN recognition method

The PD signal would unavoidably contain some noise. The sources of noise may be generated from the PD detector, the environmental electromagnetic, or the human mistakes, etc. To take into account the noise, 200 sets of testing data are created by adding the random uniformly distributed noises from ±10% to ±30%. The recognition accuracy rates with different amounts of noise added are given in Table 2. The recognition accuracy without noise added almost arrives at 100%. To demonstrate the effectiveness of the proposed method, comparative studies using a BPNN with 3 layers and 12–12–5 neurons, extension theory, and K-means algorithm are all conducted on the same testing data. The ENN recognition even has 97.8% accuracy rate in the case of ±30% noise added. The accuracy of the extension method is 93%, the BPNN is 83.8%, and the K-means algorithm is only 67.5% in the same condition. It shows that the proposed method has pretty high recognition accuracy and good tolerance to noise added. It is very encouraged to implement the proposed method in a PD detector device for real-time PD recognition.

**Table 2**
Accuracy rates of PD recognition.

| % of noise | Average recognition rate[a] (%) | | | |
|---|---|---|---|---|
| | ENN method | Extension method | MNN | K-means |
| 0 | 99 | 100 | 100 | 82 |
| ±10 | 98.9 | 99.6 | 98.5 | 73.2 |
| ±20 | 98.5 | 96.8 | 89.9 | 69.8 |
| ±30 | 97.8 | 93 | 83.8 | 67.5 |

[a] Average of 10 random trials.

## 6. Conclusions

This paper presents a new PD recognition method based on the fractal features and the ENN for PD recognition of high-voltage power apparatus. The fractal features and the mean discharges are used to highlight the more detailed characteristics of the raw 3D PD patterns. The recognition rates of the proposed method are quite high with 97.8% in extreme noise of ±30%. The experimental results indicate that this method is able to implement an efficient classification with a very high recognition rate. Compared with the MNN-based recognition method, the structure of the ENN is simpler and the learning time is faster than MNN-based method. Moreover, the proposed ENN-based recognition method also permits fast adaptive processing for a new PD defect, because it only tunes the boundaries of classified features or adds a new neural node. From the tested examples, the proposed method has a significantly high degree of recognition accuracy and shows good tolerance to noise added. This new method merits more attention to be a useful tool in PD recognition problems.

## Acknowledgement

The support of this research by the National Science Council of the Republic of China under Grant No. NSC 96-2213-E-167-029-MY3 is gratefully acknowledged.

## References

Cai, W. (1983). The extension set and incompatibility problem. *Journal of Scientific Explore, 1*, 81–93.
Chen, H. C., Gu, F. C., & Lee, C. Y. (2008). A new method based on extension theory for partial discharge pattern recognition. *WSEAS Transaction on Systems, 7*(12), 1402–1411.
Karthikeyan, B., Gopal, S., & Venkatesh, S. (2008). Partial discharge pattern classification using composite versions of probabilistic neural network inference engine. *Expert Systems with Applications, 34*(3), 1938–1947.
Karthikeyan, B., Gopal, S., & Vimala, M. (2005). Conception of complex probabilistic neural network system for classification of partial discharge patterns using multifarious inputs. *Expert Systems with Applications, 29*(4), 953–963.
Lay, Y. L. et al. (2008). The application of extension neuro-network on computer-assisted lip-reading recognition for hearing impaired. *Expert Systems with Applications, 34*(2), 1465–1473.
Li, X. et al. (2009). Fuzzy self-organizing maps for detection of partial discharge signals. In *Proceedings of IEEE/ASME international conference on advanced intelligent mechatronics* (pp. 1683–1688).
Li, J., Liao, R., Grzybowski, S., & Yang, L. (2010). Oil-paper aging evaluation by fuzzy clustering and factor analysis to statistical parameters of partial discharges. *IEEE Transactions on Dielectrics and Electrical Insulation, 17*(3), 756–763.
Mandelbrot, B. B. (1983). *The fractal geometry of nature*. New York: Freeman.
Okabe, S., Kaneko, S., Minagawa, T., & Nishida, C. (2008). Detecting characteristics of SF6 decomposed gas sensor for insulation diagnosis on gas insulated switchgears. *IEEE Transactions on Dielectrics and Electrical Insulation, 15*(1), 251–258.
Ruello, G. et al. (2010). Measurement of the electromagnetic field backscattered by a fractal surface for the verification of electromagnetic scattering models. *IEEE Transactions on Geoscience and Remote Sensing, 48*(4), 1777–1787.
Satish, L., & Zaeng, W. S. (1995). Can fractal features be used for recognizing 3-D partial discharge patterns? *IEEE Transactions on Dielectrics and Electrical Insulation, 2*, 352–359.
Voss, R. F. (1985). *Random fractal: Characterization and measurement*. New York: Plenum Press.
Wang, M. H. (2005). Partial discharge pattern recognition of current transformers using an ENN. *IEEE Transaction on Power Delivery, 20*(3), 1984–1990.
Wang, M. H., & Hung, C. P. (2003). Extension neural network. In *Proceedings of international conference on neural network* (pp. 399–403).
Wang, M. H., Tseng, Y. F., Chen, H. C., & Chao, K. H. (2009). A novel clustering algorithm based on the extension theory and genetic algorithm. *Expert Systems with Applications, 36*(4), 8269–8276.
Wu, Y. T. et al. (2010). Using 3D FFT fractal dimension estimator to analyze the complexity of fetal cortical surface from MR images. *Expert Systems with Applications, 37*(8), 6123–6127.
Yue, B. et al. (2006). Diagnosis of stator winding insulation of large generator based on partial discharge measurement. *IEEE Transactions on Energy Conversion, 21*(2), 387–395.